Slovak University of Technology in Bratislava
Faculty of Civil Engineering

Ing. Blažej Bucha

Executive summary of the dissertation thesis

GRAVITY FIELD MODELLING IN TERMS OF SPHERICAL RADIAL BASIS FUNCTIONS

to acquire the academic degree philosophiae doctor, PhD.

in the doctoral study programme 3636 geodesy and cartography

Bratislava 2016

The thesis was prepared in the full-time form of study at the Department of Theoretical Geodesy, Faculty of Civil Engineering, Slovak University of Technology in Bratislava.

PhD. student: Ing. Blažej Bucha
Department of Theoretical Geodesy
Faculty of Civil Engineering, STU in Bratislava
Radlinského 11, 810 05 Bratislava

Supervisor: doc. Ing. Juraj Janák, PhD.
Department of Theoretical Geodesy
Faculty of Civil Engineering, STU in Bratislava
Radlinského 11, 810 05 Bratislava

Oponents: prof. Ing. Pavel Novák, Ph.D.
Department of Geomatics
Faculty of Applied Sciences, UWB in Pilsen
Technická 8, 306 14 Pilsen, Czech Republic

doc. RNDr. Roman Pašteka, PhD.
Department of Applied and Environmental Geophysics
Faculty of Natural Sciences, CU in Bratislava
Mlynská dolina, pavilion G, 842 15 Bratislava

Ing. Róbert Čunderlík, PhD.
Department of Mathematics and Descriptive Geometry
Faculty of Civil Engineering, STU in Bratislava
Radlinského 11, 810 05 Bratislava

The executive summary was sent out: .....

The dissertation defence takes place .....
at the Department of Theoretical Geodesy, Faculty of Civil Engineering, Slovak University of Technology in Bratislava, Radlinského 11, 810 05 Bratislava.

.....
prof. Ing. Stanislav Unčík, PhD.
The dean of the Faculty of Civil Engineering
Slovak University of Technology in Bratislava
Radlinského 11, 810 05 Bratislava

Abstrakt

Modelovanie tiažového poľa pomocou sférických radiálnych bázových funkcií

Dizertačná práca sa zaoberá určovaním globálneho a regionálneho tiažového poľa pomocou sférických radiálnych bázových funkcií. Na výpočet sú použité dva typy dát: kinematická dráha družice GOCE a terestrické gravimetrické merania. Je ukázané, že globálne GOCE modely založené na Shannonovej radiálnej bázovej funkcii vedú prakticky k rovnako kvalitným výsledkom ako s použitím tradičných sférických harmonických funkcií. V regionálnych experimentoch bolo dosiahnuté zlepšenie približne o 10 % v spektrálnom pásme harmonických stupňov 70 – 130. V terestrickej aplikácii je vypočítaný model tiažového poľa v oblasti územia Slovenskej republiky vo veľmi vysokom priestorovom rozlíšení. Model je založený na kombinácii sférických harmonických funkcií (do stupňa 2159), sférických radiálnych bázových funkcií (do stupňa 21 600) a metóde reziduálneho terénneho modelu (2″ priestorové rozlíšenie). Kombinovaný model je testovaný pomocou GNSS/nivelačných bodov, nezávislých terestrických gravimetrických meraní, zvislicových odchýlok a vertikálnych gradientov tiažového zrýchlenia, pričom boli dosiahnuté stredné kvadratické chyby 2.7 cm, 0.53 mGal, 0.39″ a 279 E.

Contents

Preface

Accurate knowledge of the Earth's gravity field is essential in many fields of geosciences such as climatology, geophysics, oceanography or physical geodesy. And it is the last-mentioned one, physical geodesy, whose one of the main objectives is to provide state-of-the-art gravity field models. In physical geodesy, gravity field information is necessary to obtain the geoid, which is a specific equipotential surface of the Earth's gravity field best coinciding with the mean sea level. Precise knowledge of the geoid in combination with the GNSS technology significantly simplifies, for instance, the determination of physical heights. This thesis deals with global and regional gravity field determination from two different data types: the kinematic orbit of the GOCE satellite and terrestrial gravity data. To parameterize the gravity field, we utilize band-limited spherical radial basis functions (SRBFs), which enable both global and regional gravity field modelling in a unified manner.

The core of the thesis (Sects. 3 and 4) is a compilation of two journal papers. The satellite application was published in Bucha et al. (2015), while the terrestrial application was submitted (02 May 2016) to Geophysical Journal International (Bucha et al., 2016).

1 Prior research on spherical radial basis functions

Spherical radial basis functions have long been recognized as a useful mathematical tool to model the Earth's external gravity field. The studies on gravity field modelling via SRBFs go at least back to the late 1960s (e.g., Krarup, 1969). In the author's opinion, the use of SRBFs is attractive mainly because of the following properties:

1. data of different origin can directly be combined altogether (e.g., terrestrial and satellite data);
2. SRBFs can be harmonically upward continued and thus represent the external gravity field as well;
3. SRBFs enable both global and regional gravity field modelling;
4. input data do not necessarily have to be regularly spaced or refer to a regular surface such as the sphere;
5. the use of SRBFs on a regional scale substantially reduces the total number of coefficients to be determined when compared with the traditional spherical harmonics.

The methods based on SRBFs can be classified with respect to the kernel function.

1. *Point-mass kernel* (e.g., Claessens et al., 2001) – In this method, a finite number of point masses is located beneath the Earth surface in such a way that the gravity field they generate according to Newton's law of gravitation fits best (usually in the least-square sense) the input data, e.g., gravity anomalies.
2. *Radial multipoles* (e.g., Marchenko, 1998) – The method employs radial derivatives of the point-mass kernel.

3. *Least-squares collocation* (e.g., Krarup, 1969) – In the least-squares collocation, the auto-covariance function of the data, which describes stochastic behaviour of the function under consideration at two points, is used as the kernel function. The appropriate selection of the auto-covariance function is probably one of the most difficult steps of this method.
4. *Spherical wavelets* (e.g., Freeden and Schneider, 1998) – Spherical wavelets enable a decomposition of a signal (e.g., gravity anomalies, deflections of the vertical, etc.) into different spectral bands similarly as in the spherical harmonic case.

Another examples of SRBFs are Dirac approach (Bjerhammar, 1976), Poisson wavelet (e.g., Holschneider et al., 2003) or spherical splines (e.g., Alfeld et al., 1996). For further references, the reader might want to consult, among many others, Klees et al. (2008) and the references therein.

Of this somewhat wide variety of SRBF-based approaches, the one we employ benefits from the theory of spherical wavelets to a large extent. Particularly, we use band-limited SRBFs, whose the main advantage (in this author's opinion) is the possibility to decompose a signal into different frequency bands. This technique, also called the multi-resolution analysis, is not usually applied (or applicable) in the rest of the SRBF-based approaches. Working with the same signal, say with gravity anomalies, in various spectral bands is of particular importance both in geodesy and geophysics. In geodesy, one frequently needs to combine various data types, some of which may be accurate only within a specific spectral band (e.g., the gravitational gradients measured by the GOCE satellite), or needs to remove certain wavelengths of the gravity field, for instance, when applying the remove-compute-restore method. In addition to that, the spectral decomposition offers further insight into the performance of the derived model, e.g., by its validation against the same spectral band in spherical harmonic models. In geophysics, the removal of the long-wavelength features of the gravity field helps to, e.g., detect local density inhomogeneities. These useful properties of band-limited SRBFs motivated us to choose this particular SRBF-based technique.

2 Thesis objectives

The main objective of the thesis is to develop gravity field models parameterized in spherical radial basis functions from two data types: the kinematic orbit of the GOCE satellite and terrestrial gravity data.

Specific objectives:

1. Summary of the prior research on regional gravity field modelling in terms of spherical radial basis functions.
2. Development and evaluation of global and regional gravity field models from the GOCE kinematic orbit.
    - Inversion of the GOCE kinematic orbit into a gravity field model using the acceleration approach.
    - Development of global GOCE-only gravity field models and their evaluation against spherical harmonic models.

- Stabilization of zonal and near-zonal spherical harmonic coefficients of global GOCE-only gravity field models.
- Application of the acceleration approach on a regional scale and development of regional gravity field models satisfying the GOCE-only strategy.
- Mutual comparison of the global and regional GOCE-only gravity field solutions based on spherical radial basis functions.

3. Development and evaluation of a high-resolution regional gravity field model over the Slovak Republic from terrestrial gravity data.
   - Description of a combined approach to determine the regional gravity field via spherical harmonics, spherical radial basis functions and the residual terrain model technique.
   - To propose a solution to the harmonic reduction problem related to residual terrain modelling.
   - Comparison of the tesseroid- and polyhedron-based gravity forward modelling techniques in terms of the residual terrain model within the innermost zone.
   - Validation of the combined regional gravity field model against independent GNSS/levelling data, surface gravity data, deflections of the vertical and vertical gravity gradients.
   - Derivation of the second-order derivatives of spherical radial basis functions in the local north-oriented reference frame and solving the singularity-related issues.
4. To develop a software to spherical harmonic synthesis up to ultra-high degrees and orders.

3 Global and regional gravity field determination from GOCE kinematic orbit by means of spherical radial basis functions

3.1 Introduction

Kinematic orbits of low Earth orbiters proved to be a useful source of information about the long-wavelength component of the geopotential. Regarding the current and the past satellite missions, the GOCE satellite seems to be an appropriate candidate to invert its kinematic orbit into a gravity field model. The reason is twofold. First, the satellite was orbiting the Earth at an extremely low altitude ($\sim$250 km above the Earth surface), thus being more sensitive to the fine structures of the gravity field. Second, it was equipped with a geodetic-quality GPS receiver enabling a precise satellite-to-satellite tracking in the high-low mode (SST-hl). A typical feature of the GOCE mission is the Sun-synchronous orbit inclined at 96.7°. Two spherical caps of the radius $\sim$7° around the poles are therefore uncovered by the satellite ground tracks.

Gravity field models from satellite data are commonly produced on a global scale by means of spherical harmonics. Previous studies showed, however, that additional information may be extracted from these data when the gravity field is modelled on a regional scale (e.g.,

Eicker et al., 2014). Here we parameterize the gravity field by means of spatially localized basis functions, namely by spherical radial basis functions (SRBFs). A spherical radial basis function is a function on a reference sphere depending only on the spherical distance between two points on this sphere.

The aim of the present study is to deliver global and regional gravity field models from real GOCE kinematic orbit via the acceleration approach modified by Bezděk et al. (2014). We present two strategies of how to mitigate the impact of the polar gap problem, a global one and a regional one. In the global strategy, we stabilize the estimation of high-degree models (in our case of degree 130) by introducing prior information. In the second strategy, we apply the acceleration approach on a regional scale in a remove-compute-restore fashion, utilizing the long-wavelength geopotential from our global GOCE-based models.

3.2 Representation of the gravity field in terms of spherical radial basis functions

A spherical radial basis function defined on a reference sphere Ω_R is rotationally symmetric around the axis represented by the direction of the unit vector $\mathbf{r}_i/|\mathbf{r}_i|$, $\mathbf{r}_i \in \Omega_R$. Here, $\mathbf{r}_i$ is a nodal point at which the radial basis function is located and R is the radius of the sphere. Satellite data are taken at the exterior of the reference sphere Ω_R, which we shall denote as Ω_R^{ext}. The harmonic upward continuation of SRBFs into observational points is therefore of fundamental importance. It ensures that we can establish a relation between SRBFs and a gravity field quantity observed at a point $\mathbf{r} \in \overline{\Omega_R^{\text{ext}}}$, $\overline{\Omega_R^{\text{ext}}} = \Omega_R \cup \Omega_R^{\text{ext}}$. In this section, the gravity field modelling is understood in the global sense. The regional gravity field modelling will naturally follow from the global approach with only minor modifications.

The gravitational potential V at a point $\mathbf{r} \in \overline{\Omega_R^{\text{ext}}}$ expanded in a series of band-limited SRBFs reads (e.g., Freeden and Schneider, 1998)

$$V(\mathbf{r}) = \sum_{i=1}^{I} a_i \, \Phi\left(\mathbf{r}, \mathbf{r}_i\right) \, , \tag{1}$$

where $\Phi(\mathbf{r}, \mathbf{r}_i)$ is a band-limited SRBF located at the nodal point $\mathbf{r}_i \in \Omega_R$, a_i is the expansion coefficient of the ith SRBF to be determined and I is the total number of SRBFs. The band-limited SRBF is given as (Freeden and Schneider, 1998)

$$\Phi\left(\mathbf{r}, \mathbf{r}_i\right) = \sum_{n=n_{\min}}^{n_{\max}} \frac{2n+1}{4\pi \, R^2} \, \phi_n \left(\frac{R^2}{|\mathbf{r}| \, |\mathbf{r}_i|} \right)^{(n+1)} P_n\left(\frac{\mathbf{r}}{|\mathbf{r}|} \cdot \frac{\mathbf{r}_i}{|\mathbf{r}_i|} \right) \, , \tag{2}$$

where P_n is the (unnormalized) Legendre polynomial of degree n, ϕ_n are non-negative shape coefficients defining the spatial and the spectral properties of the SRBF and, finally, $n_{\min}$ and $n_{\max}$ are minimum and maximum degrees of the expansion, respectively. A SRBF is band-limited if the shape coefficients ϕ_n are zero for each degree beyond the maximum degree $n_{\max}$. If the shape coefficients ϕ_n do not vanish for infinitely many degrees, the spherical radial basis function is referred to as non-band-limited.

We use two band-limited SRBFs shown in Fig. 1:

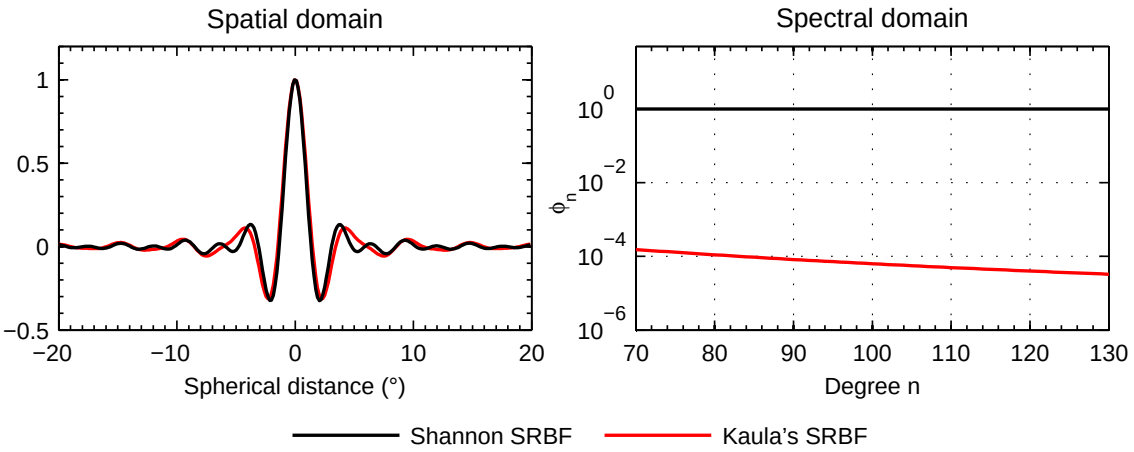

Figure 1: Spatial and spectral representations of the Shannon and Kaula's SRBFs in the spectral bandwidth $n = 70, \ldots, 130$. In Section 3.5.3, these radial basis functions are used for regional gravity field determination. The slightly smaller oscillations of Kaula's SRBF in the spatial domain are caused by the gradual attenuation of the shape coefficients ϕ_n prescribed by Kaula's rule of thumb. For a better mutual comparison in the spatial domain, the spherical radial basis functions are normalized by their values at the spherical distance of 0°.

(i) *The Shannon SRBF* defined by the shape coefficients $\phi_n = 1$ for all $n = n_{\min}, \ldots, n_{\max}$. The Shannon SRBF is the reproducing kernel of the space spanned by spherical harmonics of degrees $n_{\min}, \ldots, n_{\max}$ and all corresponding orders (Freeden and Schneider, 1998).

(ii) *SRBF based on Kaula's rule of thumb* for the degree variances of the Earth's gravitational potential (Kaula, 1966), here referred to as Kaula's SRBF. Unlike the Shannon-based models, the solutions based on Kaula's SRBF are, to some extent, forced to follow the degree variances prescribed by Kaula's rule. In Section 3.5, we therefore investigate the performance of both SRBFs.

3.3 Acceleration approach

The acceleration approach, which is based on Newton's law of motion, links the unknown expansion coefficients to the accelerations acting on the satellite. The transition from kinematic orbit to accelerations domain is performed in an inertial reference frame by applying a second-order derivative filter to the kinematic orbit. The satellite is not, however, subject solely to the gravitational force generated by the Earth. In reality, its motion is also affected by perturbing forces that need to be properly accounted for. After removing all the perturbing accelerations that can be measured on-board (non-gravitational accelerations) or modelled (direct lunisolar perturbations, accelerations due to solid Earth and ocean tides, and correction due to general relativity), the resulting accelerations acting on the spacecraft are identified with the ones caused by the geopotential.

The gravitational vector $\mathbf{g}_g$ is obtained by applying the gradient operator to the series expansion in Eq. (1),

$$\mathbf{g}_g(\mathbf{r}) = \nabla V(\mathbf{r}) = \sum_{i=1}^{I} a_i \, \nabla \Phi \left(\mathbf{r}, \mathbf{r}_i\right) \, . \tag{3}$$

After introducing random observation errors into Eq. (3), the following linear Gauss-Markov model can be established

$$\mathbf{y} = \mathbf{A}\,\mathbf{x} + \mathbf{e}\,, \quad E\{\mathbf{e}\} = \mathbf{0}\,, \quad D\{\mathbf{y}\} = \sigma^2\,\mathbf{P}^{-1}\,, \tag{4}$$

where $\mathbf{y}$ is the $N \times 1$ observation vector, $\mathbf{A}$ is the design matrix of dimensions $N \times I$, $\mathbf{x}$ is the $I \times 1$ vector of unknown expansion coefficients, $\mathbf{e}$ is the $N \times 1$ vector of stochastic observation errors, σ^2 is the (unknown) variance factor, $\mathbf{P}$ is the $N \times N$ weight matrix of the observation vector $\mathbf{y}$ and, finally, E and D denote the expectation and the dispersion operators, respectively. The design matrix in the linear model (4) is ill-conditioned and therefore some stabilization technique is necessary to obtain a unique and numerical stable solution. Following the variance components estimation approach (Koch and Kusche, 2002), a unique least-squares solution of (4) reads

$$\begin{aligned} \hat{\mathbf{x}} &= \left(\frac{1}{\sigma^2}\,\mathbf{A}^\top\,\mathbf{A} + \frac{1}{\sigma_{\boldsymbol{\mu}}^2}\,\mathbf{P}_{\boldsymbol{\mu}}\right)^{-1} \left(\frac{1}{\sigma^2}\,\mathbf{A}^\top\,\mathbf{y} + \frac{1}{\sigma_{\boldsymbol{\mu}}^2}\,\mathbf{P}_{\boldsymbol{\mu}}\,\boldsymbol{\mu}\right) \\ &= \left(\mathbf{A}^\top\,\mathbf{A} + \lambda\,\mathbf{P}_{\boldsymbol{\mu}}\right)^{-1} \left(\mathbf{A}^\top\,\mathbf{y} + \lambda\,\mathbf{P}_{\boldsymbol{\mu}}\,\boldsymbol{\mu}\right) \end{aligned} \tag{5}$$

with $\mathbf{P}_{\boldsymbol{\mu}}$ being the weight matrix of the prior information $\boldsymbol{\mu}$, $\sigma_{\boldsymbol{\mu}}^2$ is the variance factor of $\mathbf{P}_{\boldsymbol{\mu}}$ and $\lambda = \sigma^2/\sigma_{\boldsymbol{\mu}}^2$.

3.3.1 Regionally tailored regularization in terms of SRBFs

In Eq. (5), we can easily account for the regionally varying gravity field by splitting up the weight matrix $\mathbf{P}_{\boldsymbol{\mu}}$ into several matrices $\mathbf{P}_{\boldsymbol{\mu},j}$, $j = 1, \ldots, J$ (Eicker et al., 2014). First, the area in which the expansion coefficients a_i are to be estimated is divided into J areas. Subsequently, the corresponding diagonal elements of the weight matrix $\mathbf{P}_{\boldsymbol{\mu},j}$ are set to 1 if the points $\mathbf{r}_i$ belong to the jth area. The rest of the elements of the weight matrix $\mathbf{P}_{\boldsymbol{\mu},j}$ is set to zero (the diagonal as well as the off-diagonal ones). Clearly, $\sum_{j=1}^{J} \mathbf{P}_{\boldsymbol{\mu},j} = \mathbf{I}$. Eq. (5) can thus be rewritten as

$$\hat{\mathbf{x}} = \left(\mathbf{A}^\top\,\mathbf{A} + \sum_{j=1}^{J} \lambda_j\,\mathbf{P}_{\boldsymbol{\mu},j}\right)^{-1} \left(\mathbf{A}^\top\,\mathbf{y} + \sum_{j=1}^{J} \lambda_j\,\mathbf{P}_{\boldsymbol{\mu},j}\,\boldsymbol{\mu}\right) \tag{6}$$

with $\lambda_j = \sigma^2/\sigma_{\boldsymbol{\mu},j}^2$.

3.4 Data

Global and regional gravity field models to be presented in Section 3.5 are based on the GOCE kinematic orbit covering the period 01 November 2009 to 11 January 2010. Table 1 specifies the data and the background models that we employ. Furthermore, we assume that the non-gravitational accelerations in the along-track direction are to a large extent compensated by the drag-free control system. The non-gravitational accelerations in the cross-track and the radial directions are modelled, see Bezděk et al. (2014). For the validation of our results, we made use of the EIGEN-6S model (Förste et al., 2011). This model is expected to be superior to our models at least by one order of magnitude; therefore, we use it as a high-quality reference model.

Table 1: Data and background models.

Kinematic orbits	SST_PSO_2
Rotation between the inertial and the terrestrial reference frames	IERS Conventions 2010
Rotation between the inertial and the satellite-fixed reference frames	EGG_IAQ_2c
Solid Earth tides	anelastic Earth
Ocean tides	FES 2004
Lunar and solar ephemerides	JPL DE405
Neutral thermospheric density	DTM-2000
Relativistic correction	

3.5 Results

3.5.1 Global solutions free from prior information

We show in Fig. 2 a comparison between our SRBF solution complete to degree 130 and the models by Baur et al. (2014), kindly provided by Oliver Baur. These models are based on the same GOCE SST-hl data as we used, but rely on the spherical harmonic parametrization. The presence of the "zig-zag pattern" in the difference degree amplitudes, which is typical for GOCE-only models, is the strongest in our SRBF solution. In the spectral band 2–60, the even degrees are determined most weakly in the SRBF solution, while its odd degrees outperform

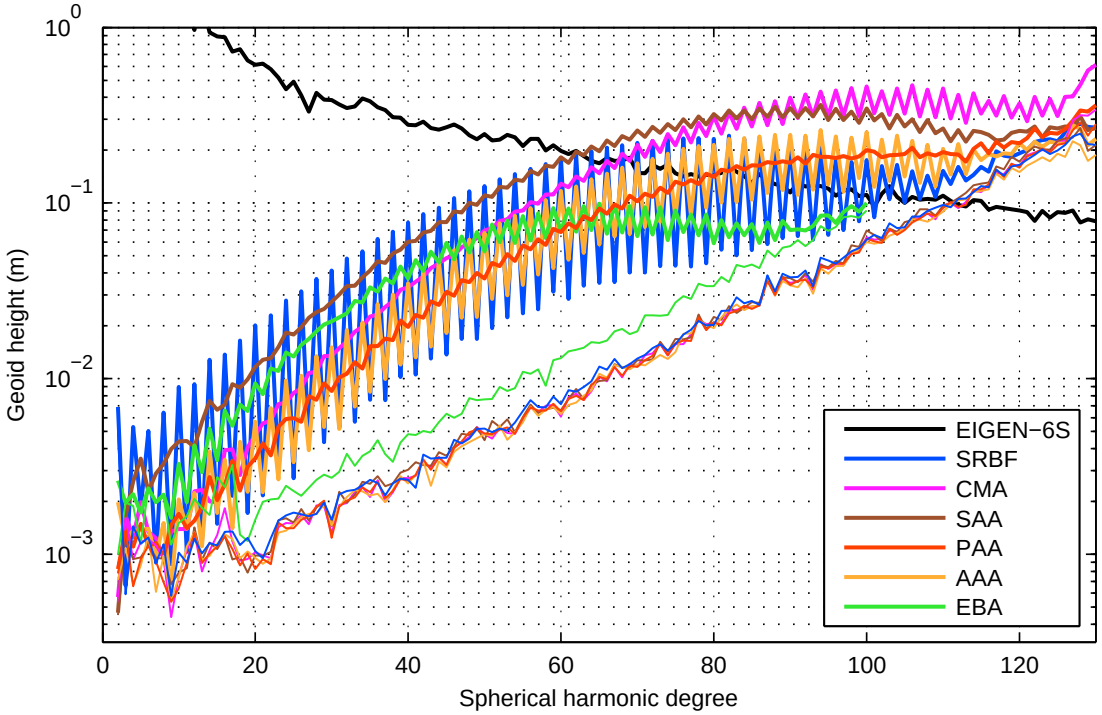

Figure 2: Difference degree amplitudes and modified difference degree amplitudes of the SRBF model to degree 130 and of the spherical harmonic models derived by: the celestial mechanics approach (CMA), the short-arc approach (SAA), the point-wise acceleration approach (PAA), the averaged acceleration approach (AAA) and the energy balance approach (EBA). Thick lines – all spherical harmonic coefficients considered; thin lines – zonal and near-zonal spherical harmonic coefficients excluded. Reference model: EIGEN-6S.

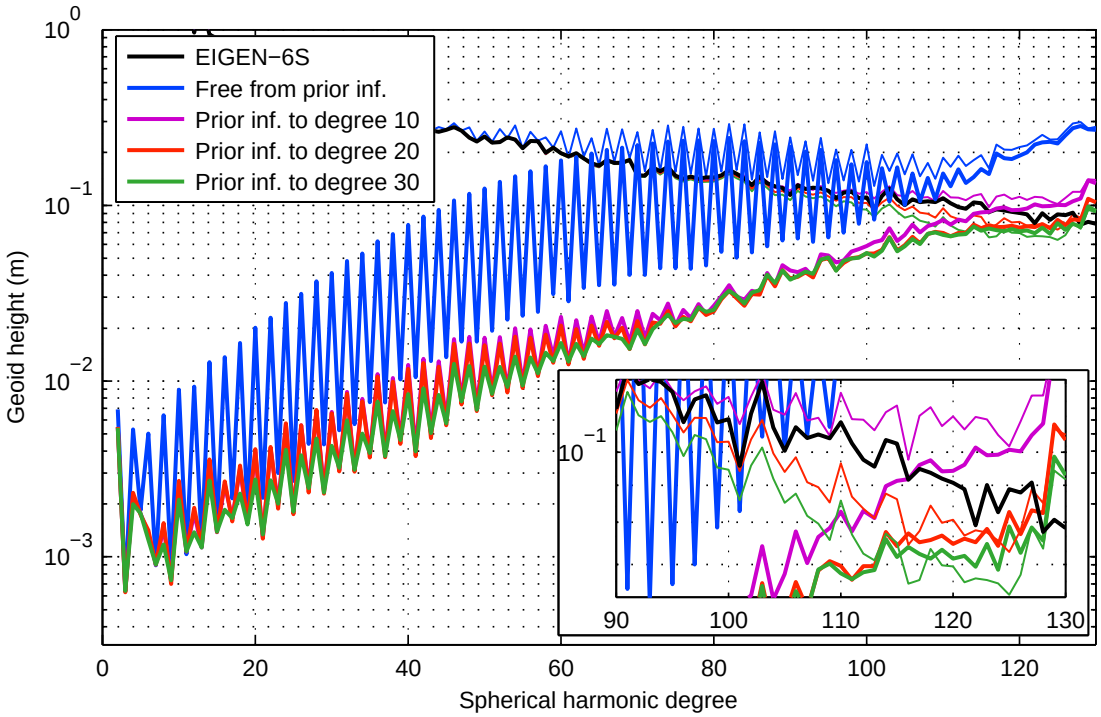

Figure 3: Difference degree amplitudes (thick lines) and signal amplitudes (thin lines) of the SRBF solutions complete to degree 130 with various prior information. In the bottom part of the spectrum, the red and the purple curves virtually overlap each other. Similarly, the red and the green curves closely follow each other for degrees beyond ∼80. The bottom right plot shows a detail on the spectral band 90–130. Reference model: EIGEN-6S.

the rest of the models nearly over all the frequencies. We assign this behaviour to the particular modification of the acceleration approach, and not to the parametrization by SRBFs. Next, we also shown in Fig. 2 modified difference degree amplitudes (the thin lines) excluding the zonal and near-zonal coefficients according to the rule of thumb proposed by Sneeuw and van Gelderen (1997). The modified version better reveals the quality of the coefficients that are almost unaffected by the polar gap problem. It can be seen that the modified difference degree amplitudes imply that our SRBF approach is able to deliver global gravity field models of comparable quality with respect to the rest of the spherical harmonic approaches.

3.5.2 Global solutions based on prior information pre-computed from GOCE

In this section, we attempt to prevent the deterioration of zonal and near-zonal spherical harmonic coefficients of GOCE-only solutions. To this end, we derive the prior information $\boldsymbol{\mu}$ from our global GOCE-only model complete to degree 75. Thanks to the low resolution of this model, its deterioration due to the polar gap problem is minor.

Figure 3 evaluates solutions complete to degree 130 with incorporated prior information to degrees $n_{\max,\mu} = 10$, 20 and 30. As a key finding of this section, we observe that the zonal and near-zonal spherical harmonic coefficients are distinctly superior to the solution free from prior information. Note that the cut-off degree $n_{\max,\mu}$ noticeably influences the final solution. The "zig-zag pattern" is to a large extent suppressed also for $n_{\max,\mu} = 10$ and 20, but the solution

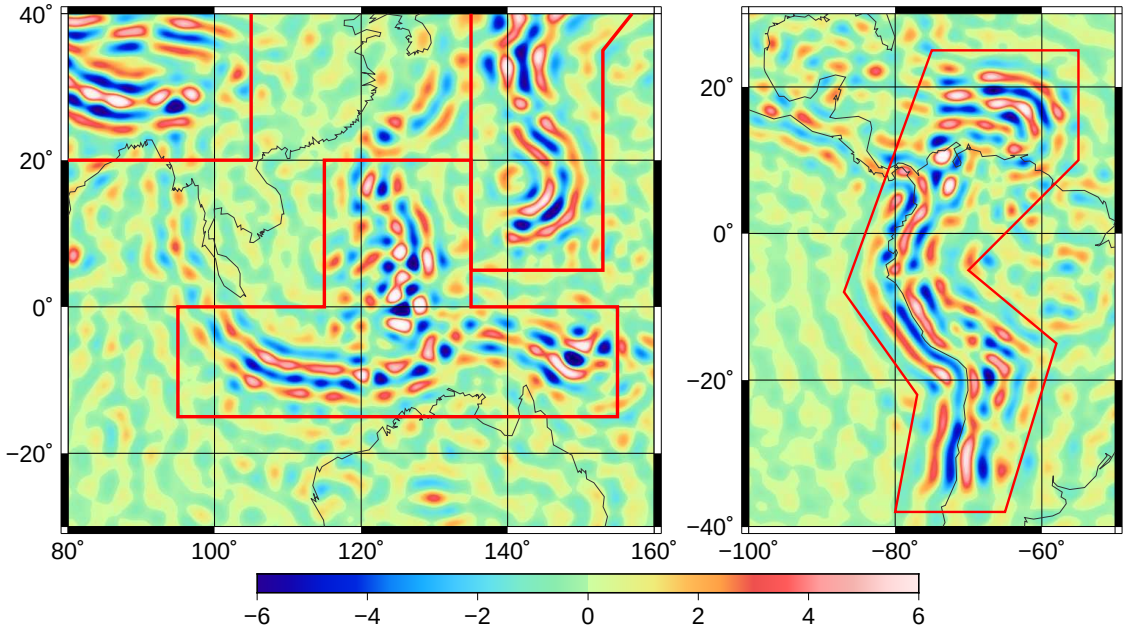

Figure 4: Geoid undulations (m) over two regions to be regionally refined, here called Indonesia (left panel) and the Andes (right panel). Indonesia: min = −12.069 m, max = 9.447 m; The Andes: min = −6.916 m, max = 8.629 m. The geoid undulations are synthesized from the EIGEN-6S reference model in the spectral band 70–130 with the grid step of 0.1° in both directions. The red lines bound the areas where separate regularization parameters will be used.

with $n_{\max,\mu} = 30$ shows the smallest difference degree amplitudes. This is achieved, however, at the cost of unintended low-pass filtering of the geopotential starting near degree 80. This effect can be seen from the thin green curve (the signal from the solution with $n_{\max,\mu} = 30$) running below the black one (the signal from the EIGEN-6S reference model). As expected, the smoothing effect decreases with decreasing the cut-off degree $n_{\max,\mu}$. For this particular case, we therefore consider the cut-off degree $n_{\max,\mu} = 10$ as a proper choice. We expect that to obtain optimum results with GOCE orbital data from a shorter/longer time period, a slightly different value of $n_{\max,\mu}$ might be required.

As far as the difference degree amplitudes are concerned, in the middle part of the spectrum, all these solutions outperform the models in Fig. 2 almost by one order of magnitude. Not shown in Fig. 3 for the sake of clarity, but within this spectral band, the modified difference degree amplitudes remain practically unchanged. The benefit of this approach is that the ratio between removing the "zig-zag pattern" and low-pass filtering of the geopotential can be well-controlled by the choice of the cut-off degree $n_{\max,\mu}$.

3.5.3 Regional solutions

In the regional gravity field modelling, we neglect all the points in kinematic orbit with ground tracks outside a given region (the data area). We aim at a regional refinement of the global models over the bandwidth 70–130. We chose two study areas, depicted in Fig. 4, where the geoid features the strongest variations between positive and negative values. We anticipate that the regionally tailored gravity field recovery method might outperform the global approach and extract some additional information about the gravity field (i.e. reduce the noise). To

prevent edge effects, the data areas are extended by 10° in each direction with respect to the study areas. The placing of the SRBFs is defined by the Reuter grid with the parameter $n_{\max} = 130$, considering only the points that fall inside the study areas extended by 20°. The long-wavelength gravity signal (degrees 0–69) is taken from our global model complete to degree 100 with $n_{\max,\mu} = 30$. As the prior information, we always use the zero vector, i.e. $\boldsymbol{\mu} = \mathbf{0}$, which is common in regional gravity field recovery.

Evaluations of the regional solutions are provided in Figure 5 and Table 2. The differences for the Kaula-based solutions (not depicted here) show virtually the same behaviour. We observe that the use of multiple regularization parameters noticeably improves the results. In particular, the RMS errors decreased by about 8–11 %. Importantly, in addition to the RMS errors, all the minimum and the maximum differences also dropped by about 10–25 %. This implies that instead of the smoothing effect achieved in Sect. 3.5.2, this time we observe an overall improvement. The regionally tailored regularization technique therefore indeed outperforms the use of a single regularization parameter.

In our experiments, the Shannon-based results systematically turn out to be slightly superior to the Kaula-based ones, since Kaula's SRBF acts as a low-pass filter (note the larger minimum and maximum differences). This is not surprising, as Kaula's rule itself suppresses certain frequencies of the gravity signal due to the underpowered geopotential within some spectral bands. Naturally, the smoothing effect mostly affects the high frequencies of the geopotential signal. This, however, contradicts one of the basic ideas upon which the regional gravity field modelling is based. That is, to regionally extract additional high-frequency gravity field features that may be difficult to detect on the global scale. We therefore prefer the Shannon SRBF, which is free from prior assumptions on the behaviour of the degree variances of the geopotential.

A mutual comparison of the signal (Fig. 4) with the discrepancies (Fig. 5) indicates a smoothing even in the Shannon-based differences. To a large extent, we attribute this behaviour to the prior information $\boldsymbol{\mu} = \mathbf{0}$. At first glance, this choice is natural, as the global residual gravity signal has a zero mean. But in this case, the impact of $\boldsymbol{\mu} = \mathbf{0}$ seems to be significant which results in a pushing the gravity signal towards the zero, i.e. the smoothing. A similar behaviour was observed in Section 3.5.2, where we used various values of the cut-off degree $n_{\max,\mu}$. The

Table 2: Differences in terms of geoid heights between the regional SRBF solutions and the EIGEN-6S in the spectral band 70–130. The differences are computed with the grid step of 0.1° in both directions. All values are in metres.

	Indonesia				The Andes			
SRBF	Min	Max	Mean	RMS	Min	Max	Mean	RMS
Regional solutions with a single regularization parameter								
Shannon	−4.442	4.563	−0.001	0.614	−3.729	4.367	−0.001	0.610
Kaula	−4.861	5.184	−0.001	0.670	−4.102	4.690	−0.001	0.664
Regional solutions with multiple regularization parameters								
Shannon	−3.715	3.753	0.000	0.563	−2.832	3.273	0.000	0.559
Kaula	−4.496	4.609	−0.001	0.610	−3.418	3.726	−0.001	0.591

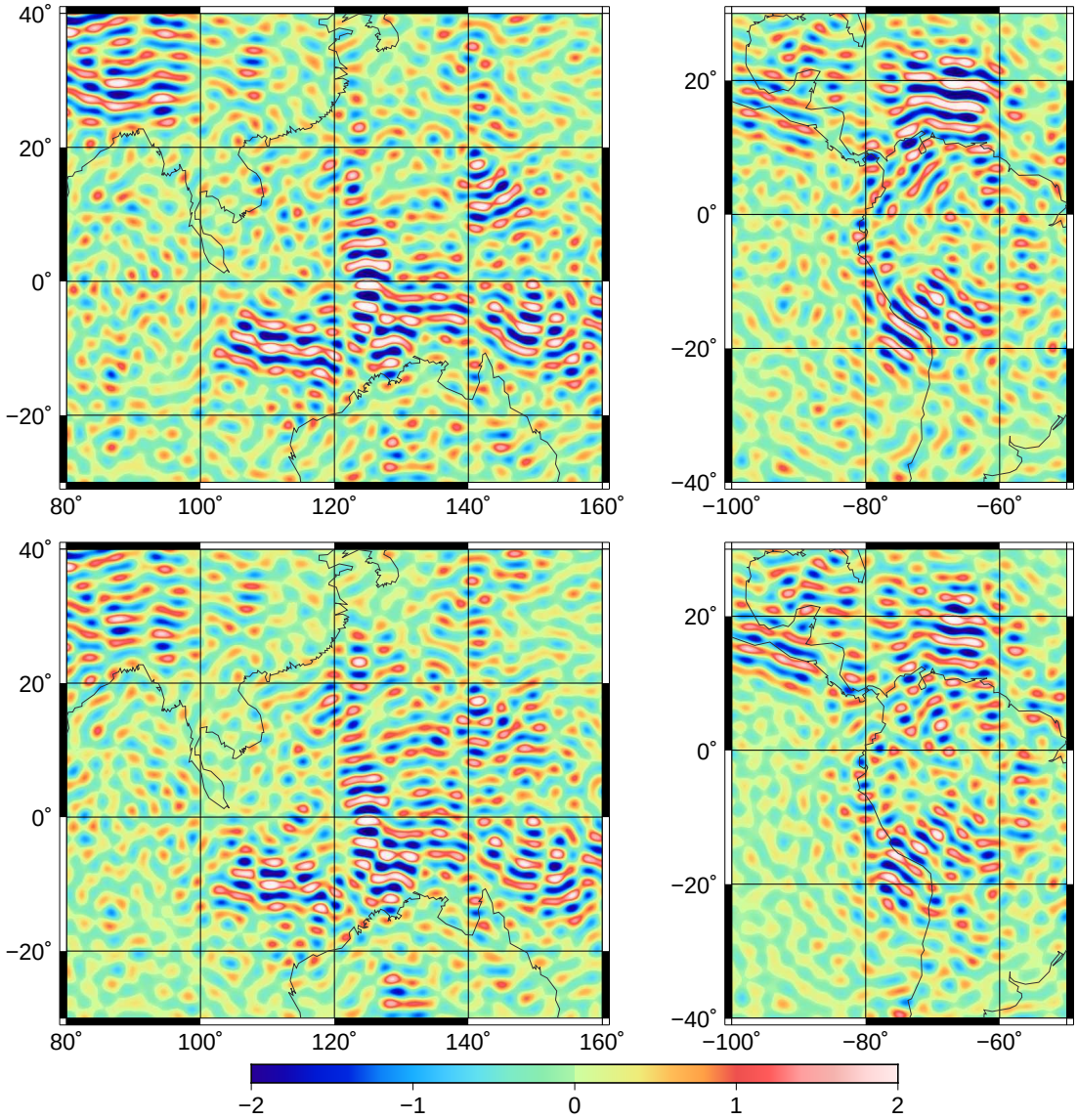

Figure 5: Geoid height differences (m) between the regional Shannon-based SRBF solutions and the EIGEN-6S in the spectral band 70–130. Upper row – regional solutions with a single regularization parameter; bottom row – regional solutions with multiple regularization parameters.

smoothing effect could be avoided or suppressed, e.g., by (i) using orbital data from a longer time period; (ii) lowering the maximum degree $n_{\max}$; (iii) choosing the prior information $\boldsymbol{\mu}$ more carefully. As for the last option, the prior information over the study area can be based, up to some cut-off degree $n_{\max,\mu}$, on the global solutions presented in Sects. 3.5.1 and 3.5.2.

4 High-resolution regional gravity field modelling in a mountainous area from terrestrial gravity data

4.1 Introduction

In recent years, significant progress has been made in gravity field modelling at very short spatial scales. One of the major breakthroughs was certainly due to the EGM2008 model (Pavlis

et al., 2012), which approximates the Earth's gravity signal down to about 9 km resolution. Though this resolution may suffice for some global applications, demands on regional gravity field knowledge are often far beyond this scale. In rugged terrain, spherical harmonic models are therefore often supplemented with high-frequency gravity information implied by the local (residual) topography using a residual terrain model (RTM, Forsberg, 1984). Despite the optimistic results achieved with high-degree harmonic models along with the RTM technique, the main limiting factor of this combination is obvious. In practice, the RTM method cannot deliver the true high-frequency gravity signal, owing to the (usually) assumed constant density of topographic masses. To achieve further improvements, the residual short-scale signal needs to be taken mainly from terrestrial data whose signal power is rich in high harmonic degrees, e.g., gravity, deflections of the vertical or vertical gravity gradients. This can be done in the remove-compute-restore fashion. The terrestrial observations, reduced by a high-degree spherical harmonic model and RTM data, can be inverted into a residual field. To model the residual component of the gravity field, we employ spherical radial basis functions.

Here we develop a regional gravity field model over the Slovak Republic (Central Europe) by means of degree-2159 harmonic models, the RTM technique and a SRBF-based approach to model the residual part from terrestrial gravity data. In this region, terrestrial gravity measurements are dense enough (3 – 6 stations per km^2, in some regions even more) to model the gravity field up to degrees as high as 21 600. These circumstances provide a good opportunity to perform high-resolution regional gravity field modelling via a combination of spherical harmonics and SRBFs. Here we use the Shannon SRBF.

4.2 Regional gravity field modelling

We use terrestrial gravity data to estimate the residual part of the regional gravity field. At first, the magnitude of the gravity vector $g(\mathbf{r})$ is projected onto the radial direction using deflections of the vertical predicted from EIGEN-6C4 (Förste et al., 2014) and the RTM. Then, we transform the obtained radial projection $g_r(\mathbf{r})$ into a residual gravity disturbance

$$\delta g_r^{res}(\mathbf{r}) = g_r(\mathbf{r}) - \gamma_r(\mathbf{r}) - \delta g_r^{SH}(\mathbf{r}) - g_r^{RTM}(\mathbf{r})\,, \tag{7}$$

where $\gamma_r(\mathbf{r})$, $\delta g_r^{SH}(\mathbf{r})$ and $g_r^{RTM}(\mathbf{r})$ are, respectively, negative values of the radial component of the normal gravity vector, of the gravity disturbance vector synthesized from a spherical harmonic model and of the RTM-implied gravitational vector. The observation equation for the residual gravity disturbance is

$$\delta g_r^{res}(\mathbf{r}) = -\sum_{i=1}^{I} a_i \frac{\partial \Phi(\mathbf{r}, \mathbf{r}_i)}{\partial r} + e \tag{8}$$

with e being the observation error. Note that the coefficients a_i now represent the residual gravity field. In vector-matrix form, Eq. (8) reads

$$\mathbf{y} = \mathbf{A}\,\mathbf{x} + \mathbf{e}\,, \tag{9}$$

where $\mathbf{y}$ is the vector of residual gravity disturbances, $\mathbf{A}$ is the design matrix, $\mathbf{x}$ is the vector of expansion coefficients and $\mathbf{e}$ is the error vector. The design matrix in the linear model (9)

is ill-conditioned (e.g., Bentel et al., 2013), thus a regularization is necessary to obtain a numerically stable solution. To this end, we apply the Tikhonov regularization along with the variance components estimation approach (see, e.g., Klees et al., 2008) to obtain the optimum regularization parameter.

4.3 Data

We use three main input data types.

1. *Gravity data* – Three terrestrial gravity data sets, here denoted as GD1, GD2 and GD3, are used. The GD1 database consists of 211 631 observations (3 – 6 stations per km^2) with an expected accuracy of ∼0.1 – 0.2 mGal. The gravity data in GD2 comprise a total of 107 416 stations with an expected accuracy of about 0.1 mGal. The third database, GD3, is a compiled grid of gravity disturbances within the area of Central Europe with the step of 20 and 30 arcsec in ellipsoidal latitude and longitude, respectively. In this database, the gravity stations outside the Slovak Republic are of poor quality (∼2 mGal), and therefore are only used to reduce edge effects, i.e. several kilometres beyond the boundary of the Slovak Republic
2. *Global spherical harmonic models* – The long and medium wavelengths of the gravity field are modelled by EIGEN-6C4 up to its maximum harmonic degree 2190. Some of the computations are also performed with EGM2008.
3. *Topographic models* – We approximate the topography by a national topographic model DMR-3.5 at the spatial resolution of 2 arcsec, kindly provided by the Geodetic and Cartographic Institute Bratislava. The reference topography is represented by the spherical-harmonic-based model DTM2006.0 (Pavlis et al., 2007) truncated at degree 2159.

For the validation purposes, we make use of four various gravity field quantities: the height anomaly derived from GNSS/levelling data, the gravity, the astrogeodetic deflection of the vertical and the vertical gravity gradient. These data types mutually complement each other and thus enable validation from different perspectives. We use five data sets, some of which are shown in Fig. 6.

1. *GNSS/levelling data* – The control GNSS/levelling points are divided into two sets, GL1 and GL2. The GL1 set consists of 347 control points with an accuracy of the height anomaly better than 2 cm. In the GL2 data set, 61 points of a slightly lower accuracy than in GL1 (∼2 cm) are grouped together. For the sake of clarity, the GL1 points are not depicted in Fig. 6, but will be shown later.
2. *Independent gravity data* – 1264 gravity stations with an accuracy better than 0.02 mGal are used as a next data set GD4 (also shown later).
3. *Astrogeodetic deflections of the vertical* – This data set, hereafter denoted as DV, consists of 64 pairs of astrogeodetic deflections of the vertical with an expected accuracy of ∼0.2 – 0.3 arcsec. Note that this data set does not cover the whole territory. Instead, the observations are located mainly in the roughest part of the country, and thus may provide a valuable information on the local quality of the solution.

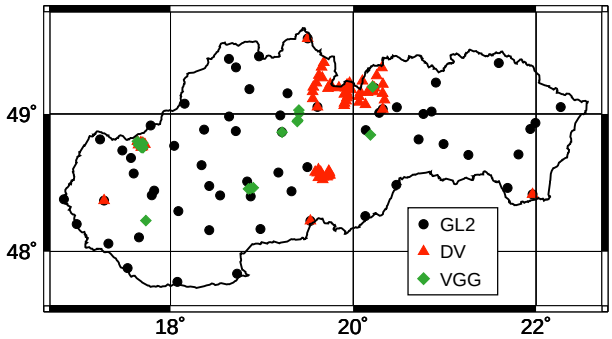

Figure 6: Spatial distribution of some of the test data sets. The position of GL1 and GD4 is shown in Figs. 9 and 10, respectively.

4. *Terrestrial vertical gravity gradients* – Being the second-order derivative of the gravity potential, vertical gravity gradients possess a strong signal power in high frequencies and therefore may well serve for validating a high-resolution gravity field model. In total, 20 terrestrial vertical gravity gradients comprise the last data set VGG, see Fig. 6. Its accuracy is estimated to ∼50 E ($1\,\mathrm{E} = 10^{-9}\,\mathrm{s}^{-2}$).

4.4 Results

Regional gravity field solutions

We use a total of 351 246 gravity stations to derive the residual component of the gravity field. To reduce edge effects, the data from the GD3 database are taken up to the spherical distance of 0.085° from the borders which is slightly more than the spatial resolution of degree-2159 spherical harmonic models. Since we expect different quality of the input gravity databases, each one is treated as a separate observation group with its own variance factor to be determined by the variance components estimation approach. The spatial distribution of the input data enables to expand the residual gravity field up to degree $n_{\max} = 21\,600$ correspoding to 30 arcsec spatial resolution. The spatial distribution of the points $\mathbf{r}_i \in \Omega_R$ is defined by the Reuter grid with the parameter $n_{\max}+1$. Of this grid, only the points up to the spherical distance of 0.125° from the borders are used. Note that the points $\mathbf{r}_i$ slightly exceed the data area in order to improve the least-squares fit. The value 0.125° was found empirically. The total number of the points $\mathbf{r}_i$, and thus also of the expansion coefficients, is 77 769. EIGEN-6C4 up to its maximum degree 2190 is used to model the long and medium wavelengths of the gravity field.

In Table 3, we show the statistics of the least-squares residuals using $n_{\min} = 0$ and $n_{\min} = 2160$ in the series expansion of SRBFs (see Eq. 2). The residuals related to the GD1 database are depicted in Fig. 7. Though the signal from EIGEN-6C4 was removed from the input gravity data, the least-squares residuals for $n_{\min} = 2160$ clearly imply that the harmonic degrees below 2160 are still present in the input residual gravity disturbances.

To examine this issue, we performed a spectral decomposition (see, e.g., Freeden and Schneider, 1998) of the residual gravity disturbances in spherical approximation (the negative first-order radial derivative of the residual potential) synthesized from the estimated expansion coefficients ($n_{\min} = 0$), see Fig. 8. We decomposed the signal into 6 spectral bands: 3 bands

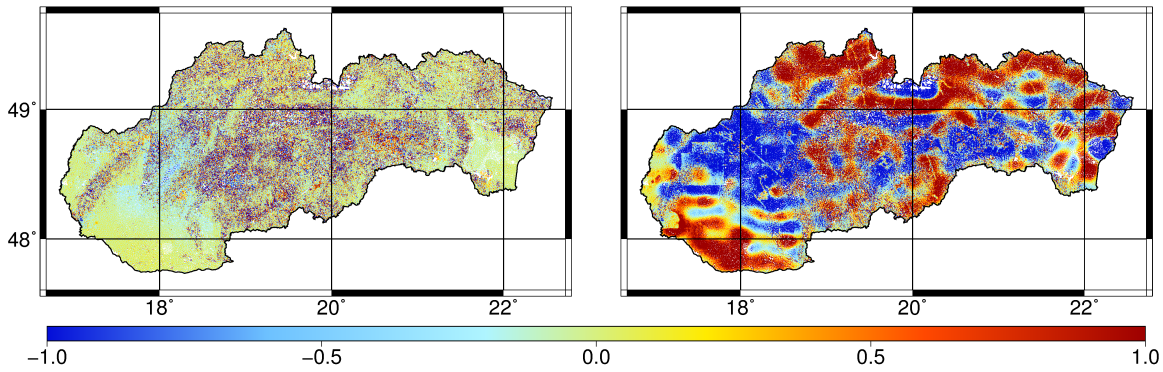

Figure 7: Least-squares residuals (mGal) related to the GD1 database using $n_{\min} = 0$ (upper panel) and $n_{\min} = 2160$ (bottom panel). See Table 3 for the statistics.

to degree 2159 (0 – 539, 540 – 1079, 1080 – 2159) and 3 bands beyond that degree (2160 – 5399, 5400 – 10 799 and 10 800 – 21 600). The residual signal below degree 2160 originates mainly from inaccuracies in the input gravity data, EIGEN-6C4 and the RTM-implied signal. In Section 4.4.1, each evaluation using independent data leads to a conclusion that the most dominant part of this signal seems to be due to the errors in EIGEN-6C4 and the RTM, while the errors of the input gravity data are expected to play a minor role, mostly of a high-frequency nature. This implies that, in this particular case, the series expansion in Eq. (2) should start at a lower degree than 2160 in order to absorb this useful part of the signal. This step, in turn, results in a better solution as will be shown in Section 4.4.1. Instead of deciding which value of $n_{\min}$ should be used, we simply put $n_{\min} = 0$, though it is clear that harmonic degrees below, say, 180 cannot be properly retrieved from such a small area.

The standard deviations obtained by the variance components estimation approach read (the solution with $n_{\min} = 0$) $\hat{\sigma}_1 = 0.74$ mGal, $\hat{\sigma}_2 = 0.73$ mGal and $\hat{\sigma}_3 = 4.0$ mGal. These estimates confirm that, as expected, the quality of the GD3 database is significantly lower when compared with GD1 and GD2 (see Section 4.3).

Table 3: Statistics of the least-squares residuals using $n_{\min} = 0$ and $n_{\min} = 2160$ in Eq. (2). The last column shows the percentage of the residuals falling into the mGal-level.

Data set	min (mGal)	max (mGal)	mean (mGal)	RMS (mGal)	−1 to 1 mGal (%)
	Solution with $n_{\min} = 0$				
GD1	−14.191	19.900	−0.056	0.666	90
GD2	−25.476	27.530	−0.026	0.709	92
GD3	−27.639	27.191	−1.308	3.699	34
	Solution with $n_{\min} = 2160$				
GD1	−18.108	20.313	−0.087	1.374	64
GD2	−25.691	26.785	−0.197	0.930	82
GD3	−45.068	31.733	−2.662	6.770	17

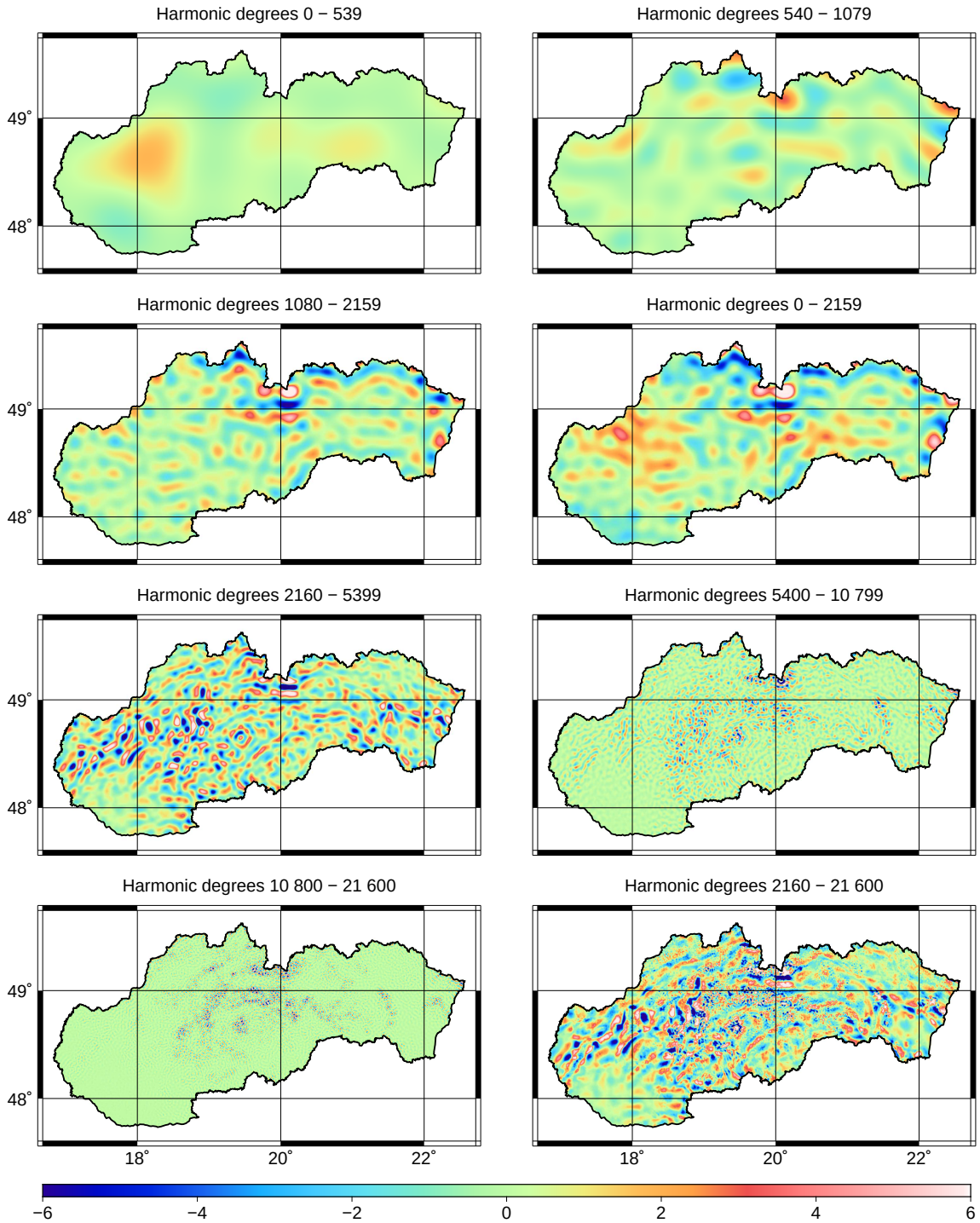

Figure 8: Spectral decomposition of residual gravity disturbances in spherical approximation (mGal) synthesized from the expansion coefficients estimated with $n_{\min} = 0$ in Eq. (2).

4.4.1 Evaluation of the regional gravity field models using independent data

GNSS/leveling data

The statistics of the differences between the height anomalies derived from the combined model and from the GNSS/levelling data are reported in Table 4. It can be seen that the RTM data and the SRBF-based part of the model improve the height anomalies at the GL1 points by 25 %. In the case of the GL2 data set, the gain in accuracy is on a negligible level if taking into

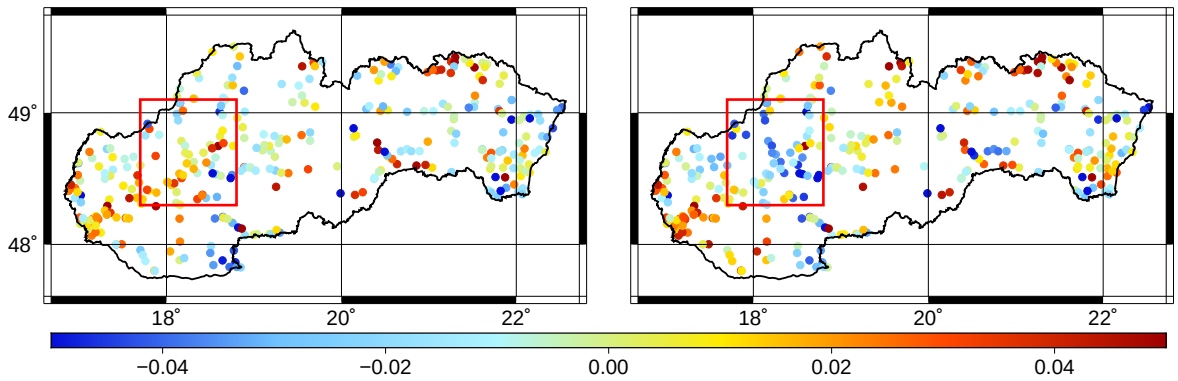

Figure 9: Differences (m) between the predicted and GNSS/levelling-based height anomalies at the GL1 data set. Upper panel – solution with $n_{\min} = 0$, bottom panel – solution with $n_{\min} = 2160$. The statistics are reported in Table 4. The red lines bound the area where the residual signal below degree 2160 clearly improves the solution (see also the same area in Fig. 8 in the spectral band of degrees 0 – 539).

Table 4: Statistics of the differences between the predicted and GNSS/levelling-based height anomalies after the removal of the constant bias term.

Variant	min (m)	max (m)	STD (m)
	The GL1 data (347 points)		
EIGEN-6C4	−0.164	0.099	0.036
EIGEN-6C4 + RTM	−0.114	0.106	0.031
EIGEN-6C4 + RTM + the Shannon SRBF ($n_{\min} = 0$)	−0.112	0.115	**0.027**
EIGEN-6C4 + RTM + the Shannon SRBF ($n_{\min} = 2160$)	−0.111	0.107	0.030
	The GL2 data (61 points)		
EIGEN-6C4	−0.098	0.141	0.036
EIGEN-6C4 + RTM	−0.094	0.096	**0.034**
EIGEN-6C4 + RTM + the Shannon SRBF ($n_{\min} = 0$)	−0.110	0.087	0.035
EIGEN-6C4 + RTM + the Shannon SRBF ($n_{\min} = 2160$)	−0.094	0.094	**0.034**

account the accuracy of this data set (∼2 cm). The large number of control points in the GL1 data set provides a good opportunity to identify whether our solutions (or the GNSS/levelling data) suffer from systematic deformations. In Fig. 9, we show the differences achieved with our two combined models. It can be seen that some of the long-wavelength features in the solution with $n_{\min} = 2160$ are slightly reduced when using $n_{\min} = 0$.

Independent gravity data

The statistics of the differences are reported in Table 5. We observe that the RTM-implied gravity signal improves the gravity from EIGEN-6C4 by ∼83 % in terms of the RMS error. After further adding the SRBF-based part of the signal ($n_{\min} = 0$), the improvement rate is of about 97 %. Clearly, the solution with $n_{\min} = 2160$ is inferior to the one with $n_{\min} = 0$ which can also be seen from Fig. 10. Note that the long-wavelength character of the discrepancies shown in the bottom panel of Fig. 10 is very similar, but of opposite sign, to that of the correction signal (harmonic degrees 0 – 2159 in Fig. 8). Since the GD4 database is composed

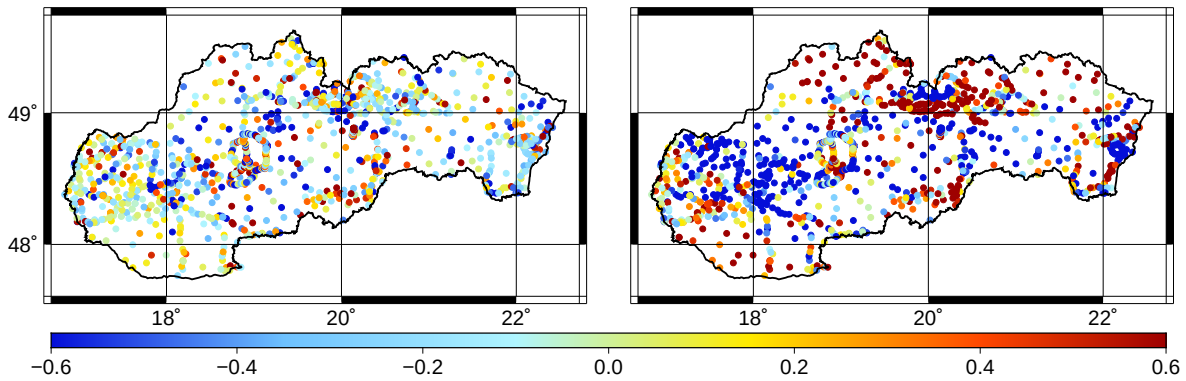

Figure 10: Differences (m) between the predicted and independent gravity at the GD4 data set. Upper panel – solution with $n_{\min} = 0$, bottom panel – solution with $n_{\min} = 2160$. The statistics are reported in Table 5.

Table 5: Statistics of the differences between the predicted and independent gravity data.

Variant	min (mGal)	max (mGal)	mean (mGal)	RMS (mGal)
	The GD4 data set (1264 observations)			
EIGEN-6C4	−61.851	80.078	6.815	17.091
EIGEN-6C4 + RTM	−13.715	8.376	−0.379	2.862
EIGEN-6C4 + RTM + the Shannon SRBF ($n_{\min} = 0$)	−3.578	3.945	−0.090	**0.526**
EIGEN-6C4 + RTM + the Shannon SRBF ($n_{\min} = 2160$)	−8.192	7.393	−0.223	1.359

of high-quality terrestrial gravity data and is completely independent from the GD1, GD2 and GD3 databases, this provides a strong evidence that, as claimed in Section 4.4, this signal is due to the inaccuracies in EIGEN-6C4 and in the RTM, and it does not originate from the input gravity data in GD1 or GD2.

Deflections of the vertical

The statistics of the differences between the synthesized and observed vertical deflections are shown in Table 6. After adding the the RTM-effect and the SRBF-based part of the model, we achieved an improvement rate of ∼80 %. The solution with $n_{\min} = 0$ is again substantially superior to that with $n_{\min} = 2160$. It has to be noted that, similarly as in the case of height anomalies, the RMS error of the differences ($n_{\min} = 0$) approaches the expected accuracy of the observations (∼0.2 – 0.3 arcsec).

Vertical gravity gradients

The statistics of the differences between the synthesized and observed vertical gravity gradients are reported in Table 7. It can be seen that the RMS error dropped by about 70 % after adding the RTM contribution, but only a negligible improvement is achieved when further including the SRBF-based part of the combined model. This is not surprising given that the vertical gravity gradient is a highly terrain-sensitive quantity.

Table 6: Statistics of the differences between the predicted and observed deflections of the vertical.

Variant	min (arcsec)	max (arcsec)	mean (arcsec)	RMS (arcsec)
	The DV data set (64 values of ξ)			
EIGEN-6C4	−3.568	6.316	−0.127	2.184
EIGEN-6C4 + RTM	−1.688	2.440	−0.134	0.712
EIGEN-6C4 + RTM + the Shannon SRBF ($n_{\min} = 0$)	−1.015	0.922	−0.036	**0.366**
EIGEN-6C4 + RTM + the Shannon SRBF ($n_{\min} = 2160$)	−1.597	1.603	−0.103	0.583
	The DV data set (64 values of η)			
EIGEN-6C4	−7.815	3.769	0.415	1.966
EIGEN-6C4 + RTM	−1.203	1.617	0.247	0.627
EIGEN-6C4 + RTM + the Shannon SRBF ($n_{\min} = 0$)	−0.673	1.159	0.111	**0.419**
EIGEN-6C4 + RTM + the Shannon SRBF ($n_{\min} = 2160$)	−1.039	1.490	0.215	0.561

Table 7: Statistics of the differences between the predicted and observed vertical gravity gradients.

Variant	min (E)	max (E)	mean (E)	RMS (E)
	The VGG data set (20 observations)			
EIGEN-6C4	−2619.7	1239.3	−297.2	913.7
EIGEN-6C4 + RTM	−775.9	322.4	−151.3	280.3
EIGEN-6C4 + RTM + the Shannon SRBF ($n_{\min} = 0$)	−766.7	315.5	−152.6	**279.3**
EIGEN-6C4 + RTM + the Shannon SRBF ($n_{\min} = 2160$)	−770.9	319.1	−157.7	280.8

5 Contribution of the thesis

1. We have shown that, while using the same data and processing strategy, regional solutions from the GOCE orbit may outperform the global ones by about 10 % in terms of the RMS error (geoid height).
2. We have proposed and applied an approach to stabilize the estimation of zonal and near-zonal spherical harmonic coefficients of global GOCE-only gravity field models.
3. We have developed a high-resolution regional gravity field model over the Slovak republic.
4. We have derived correction spherical harmonic coefficients improving the EGM2008 and EIGEN-6C4 models over the area of the Slovak Republic.
5. We have derived the second-order derivatives of spherical radial basis functions in the LNOF, and provided the formulae in a numerically stable form, which avoids the singularity-related issues.
6. We have developed and made publicly available two Matlab-based programs: GrafLab (GRAvity Field LABoratory; Bucha and Janák, 2013) and isGrafLab (Irregular Surface GRAvity Field LABoratory; Bucha and Janák, 2014). The former is designed to perform spherical harmonic synthesis up to ultra-high degrees point-wise and at grids referring to a regular surface (a sphere or an ellipsoid of revolution). The latter offers an efficient grid-wise synthesis at irregular surfaces, e.g., the Earth's surface.

6 Concluding remarks

We have shown that gravity field modelling via band-limited SRBFs is able to produce solutions of comparable or better quality than the commonly used spherical harmonics or numerical integration techniques. Particularly, we have shown that if the same input data and processing strategy are employed, the Shannon SRBF provides global gravity field models of essentially the same quality as spherical harmonics. This result is not surprising, given that it can be shown that global gravity field modelling by spherical harmonics and by the Shannon SRBF yields, in theory, the same results. But, to the best knowledge of the author, such a straightforward comparison as done here is not provided in the literature. Next, we have proposed and applied an approach to stabilize the estimation of (near-)zonal spherical harmonic coefficients of GOCE-only solutions which are usually estimated weakly. Finally, we have shown that regional solutions from the GOCE kinematic orbit may outperform the global ones by about 10 %. This improvement is shown to be mainly due to the regionally tailored regularization strategy, which is based on multiple regularization parameters.

In the terrestrial application, we have derived a regional gravity field model over the Slovak Republic which improves EGM2008 and EIGEN-6C4 substantially. In particular, we have shown that our combined model outperforms EIGEN-6C4 in the range from 25 % (height anomalies) to 97 % (gravity). Some topics and issues should be addressed in the future to achieve further enhancement. (i) It is the opinion of the author that the national digital topographic model DMR-3.5 does not meet the current demands on the knowledge of the topography in terms of both accuracy and spatial resolution. A high-quality digital topographic model is of utmost importance in order to improve the short-scale properties of the combined model, as the very short wavelengths of the gravity field are correlated with local topography to a large extent. Note that, beyond the 30 arcsec spatial resolution, our combined gravity field model relies solely on the topography-based information. The use of a topographic model of higher quality should therefore be the first candidate to improve the combined model. (ii) To validate quasigeoid solutions from terrestrial gravity data, we recommend to prefer the GL1 database over the usual GL2 in the future. Our results imply that the GL1 set is of higher overall quality than GL2. Moreover, the GL1 data set consists of $\sim$5.5 times more GNLSS/leveling points than GL2 which helps to better identify potential systematic deformations of the solution. Next, our quasigeoid solution indicates that there might be a few outliers in the GL1 data set. We therefore recommend to identify these outliers either by field measurements or by using several high-quality quasigeoid solutions developed independently, and than to remove these outliers from the database. (iii) Finally, the fact that terrestrial gravity data possess a strong signal power in high harmonic degrees motivates us to carry out numerical tests also with non-band-limited spherical radial basis functions.

References

Alfeld, P., Neamtu, M., and Schumaker, L. L. (1996). Fitting scattered data on sphere-like surfaces using spherical splines. *Journal of Computational and Applied Mathematics*, 73:5–43.

Baur, O., Bock, H., Höck, E., Jäggi, A., Krauss, S., Mayer-Gürr, T., Reubelt, T., Siemes, C., and Zehentner, N. (2014). Comparison of GOCE-GPS gravity fields derived by different approaches. *Journal of Geodesy*, 88:959–973. doi: 10.1007/s00190-014-0736-6.

Bentel, K., Schmidt, M., and Denby, C. R. (2013). Artifacts in regional gravity representations with spherical radial basis functions. *Journal of Geodetic Science*, 3:173–187. doi: 10.2478/jogs-2013-0029.

Bezděk, A., Sebera, J., Klokočník, J., and Kostelecký, J. (2014). Gravity field models from kinematic orbits of CHAMP, GRACE and GOCE satellites. *Advances in Space Research*, 53:412–429. doi: 10.1016/j.asr.2013.11.031.

Bjerhammar, A. (1976). A Dirac approach to physical geodesy. *Zeitschrift für Vermessungswesen*, 101:41–44.

Bucha, B., Bezděk, A., Sebera, J., and Janák, J. (2015). Global and regional gravity field determination from GOCE kinematic orbit by means of spherical radial basis functions. *Surveys in Geophysics*, 36:773–801. doi: 10.1007/s10712-015-9344-0.

Bucha, B. and Janák, J. (2013). A MATLAB-based graphical user interface program for computing functionals of the geopotential up to ultra-high degrees and orders. *Computers and Geosciences*, 56:186–196. doi: 10.1016/j.cageo.2013.03.012.

Bucha, B. and Janák, J. (2014). A MATLAB-based graphical user interface program for computing functionals of the geopotential up to ultra-high degrees and orders: Efficient computation at irregular surfaces. *Computers and Geosciences*, 66:219—-227. doi: 10.1016/j.cageo.2014.02.005.

Bucha, B., Janák, J., Papčo, J., and Bezděk, A. (2016). High-resolution regional gravity field modelling in a mountainous area from terrestrial gravity data. *Geophysical Journal International*. Submitted.

Claessens, S. J., Featherstone, W. E., and Barthelmes, F. (2001). Experiences with point-mass gravity field modelling in the Perth region. *Geomatics Research Australasia*, 75:53–86.

Eicker, A., Schall, J., and Kusche, J. (2014). Regional gravity modelling from spaceborne data: Case studies with GOCE. *Geophysical Journal International*, 196:1431–1440. doi: 10.1093/gji/ggt485.

Forsberg, R. (1984). A study of terrain reductions, density anomalies and geophysical inversion methods in gravity field modelling. Report No. 355, Department of Geodetic Science and Surveying, The Ohio State University, Columbus, Ohio, 129 pp.

Förste, C., Bruinsma, S., Shako, R., Marty, J.-C., Flechtner, F., Abrikosov, O., Dahle, C., Lemoine, J.-M., Neumayer, H., Biancale, R., Barthelmes, F., König, R., and Balmino, G. (2011). EIGEN-6 A new combined global gravity field model including GOCE data from the collaboration of GFZ-Potsdam and GRGS-Toulouse. In *EGU General Assembly*, Vienna, Austria, 3–8 April.

Förste, C., Bruinsma, S. L., Abrikosov, O., Lemoine, J.-M., Schaller, T., Götze, H.-J., Ebbing, J., Marty, J. C., Flechtner, F., Balmino, G., and Biancale, R. (2014). EIGEN-6C4 The latest combined global gravity field model including GOCE data up to degree and order 2190 of GFZ Potsdam and GRGS Toulouse. In *5th GOCE User Workshop*, Paris, France, 25–28 November.

Freeden, W. and Schneider, F. (1998). An integrated wavelet concept of physical geodesy. *Journal of Geodesy*, 72:259–281.

Holschneider, M., Chambodut, A., and Mandea, M. (2003). From global to regional analysis of the magnetic field on the sphere using wavelet frames. *Physics of the Earth and Planetary Interiors*, 135:107–124. 10.1016/S0031-9201(02)00210-8.

Kaula, W. M. (1966). *Theory of Satellite Geodesy: Applications of Satellites to Geodesy*. Waltham, Blaisdell, Mineola, New York, 124 pp.

Klees, R., Tenzer, R., Prutkin, I., and Wittwer, T. (2008). A data-driven approach to local gravity field modelling using spherical radial basis functions. *Journal of Geodesy*, 82:457–471. doi: 10.1007/s00190-007-0196-3.

Koch, K. R. and Kusche, J. (2002). Regularization of geopotential determination from satellite data by variance components. *Journal of Geodesy*, 76:259–268. doi: 10.1007/s00190-002-0245-x.

Krarup, T. (1969). A contribution to the mathematical foundation of physical geodesy. Meddelelse No. 44, Geodætisk Institut, København.

Marchenko, A. N. (1998). *Parameterization of the Earth's Gravity Field: Point and Line Singularities*. Astronomical and Geodetic Society, Lviv, Ukraine, 208 pp.

Pavlis, N. K., Factor, J. K., and Holmes, S. A. (2007). Terrain-related gravimetric quantities computed for the next EGM. In *Proceedings of the 1st International Symposium of the International Gravity Field Service vol. 18*, Harita Dergisi, Istanbul, 318–323.

Pavlis, N. K., Holmes, S. A., Kenyon, S. C., and Factor, J. K. (2012). The development and evaluation of the Earth Gravitational Model 2008 (EGM2008). *Journal of Geophysical Research*, 117(B04406):1–38. doi: 10.1029/2011JB008916.

Sneeuw, N. and van Gelderen, M. (1997). The polar gap. In Sansò, F. and Rummel, R., editors, *Geodetic Boundary Value Problems in View of the One Centimeter Geoid*, volume 65 of *Lecture Notes in Earth Sciences*, pages 559–568. Springer.

Publications of the author

Journal articles (refereed)

Bucha, **B.**, Janák, J., Papčo, J., Bezděk, A.: High-resolution regional gravity field modelling in a mountainous area from terrestrial gravity data. *Geophysical Journal International*, **under review**.

Bucha, **B.**, Bezděk, A., Sebera, J., Janák, J., 2015: Global and regional gravity field determination from GOCE kinematic orbit by means of spherical radial basis functions. *Surveys in Geophysics*, 36:773–801. doi: 10.1007/s10712-015-9344-0.

Kostelecký, J., Klokočník, J., **Bucha**, **B.**, Bezděk, A., Förste, C., 2015: Evaluation of the gravity field model EIGEN-6C4 in comparison with EGM2008 by means of various functions of the gravity potential and by GNSS/levelling. *Geoinformatics FCE CTU*, 14:7-–28. doi: 10.14311/gi.14.1.1.

Bucha, **B.**, Janák, J., 2014: A MATLAB-based graphical user interface program for computing functionals of the geopotential up to ultra-high degrees and orders: Efficient computation at irregular surfaces. *Computers and Geosciences*, 66:219–227. doi: 10.1016/j.cageo.2014.02.005.

Bucha, **B.**, Janák, J., 2013: A MATLAB-based graphical user interface program for computing functionals of the geopotential up to ultra-high degrees and orders. *Computers and Geosciences*, 56:186-–196. doi: 10.1016/j.cageo.2013.03.012.

Conference articles (refereed)

Bucha, **B.**, 2015: A short note on the empirical rule formulated by Hirt and Kuhn (2014). In: *Advances in architectural, civil and environmental engineering: 25th Annual PhD Student Conference on Architecture and Construction Engineering, Building Materials, Structural Engineering, Water and Environmental Engineering, Transportation Engineering, Surveying, Geodesy, and Applied Mathematics*, Bratislava, Slovakia, October 28, p. 163–164, ISBN 978-80-227-4514-7.

Bucha, **B.**, 2014: On the use of the acceleration approach to determine long-wavelength part of the gravity field parameterized in spherical radial basis functions. In: *Advances in Architectural, Civil and Environmental Engineering: 24th Annual PhD Student Conference on Architectural and Construction Engineering, Building Materials, Structural Engineering, Water and Environmental Engineering, Transportation Engineering, Surveying, Geodesy, and Applied Mathematics*, Bratislava, Slovakia, October 29, p. 142–149, ISBN 978-80-227-4301-3.

Bucha, **B.**, 2013: Analysis and synthesis of functionals of the geopotential in terms of ellipsoidal harmonic functions. In: *Advances in Architectural, Civil and Environmental Engineering: 23rd Annual PhD student conference*, Bratislava, Slovakia, October 30, p. 140–148 (in Slovak), ISBN 978-80-227-4102-6.

Abstracts

Bucha, **B.**, Bezděk, A., Janák, J., 2014: Global gravity field determination from kinematic orbits of CHAMP, GRACE and GOCE satellites by means of spherical radial basis functions. In: *Geomatika v projektech 2014 : sborník abstraktů příspěvků ze semináře*, Zámek Kozel, Czech Republic, October 1–2, p. 87–88, ISBN 978-80-263-0796-9.

Bucha, **B.**, Bezděk, A., 2015: Development and evaluation of global geopotential models derived from satellite orbits by means of spherical radial basis functions. In: *Juniorstav 2015: 17. odborná konference doktorského studia. Sborník abstraktů*, Brno, Czech Republic, January 29, p. 334, ISBN 978-80-214-5091-2.

Bucha, **B.**, Bezděk, A., Janák, J., 2015: An approach to stabilize the estimation of global GOCE-only gravity field models from kinematic orbit in terms of spherical radial basis functions. In: *Geodetické základy a geodynamika 2015: zborník príspevkov a abstraktov*, Kočovce, Slovakia, October 8–9, p. 55, ISBN 978-80-227-4466-9.

Kostelecký, J., Klokočník, J., **Bucha**, **B.**, 2015: Evaluation of EIGEN-6C4 by means of various functions of the gravitational potential and by GNSS/levelling. In: *Geodetické základy a geodynamika 2015: zborník príspevkov a abstraktov*, Kočovce, Slovakia, October 8–9, p. 65, ISBN 978-80-227-4466-9.

Papčo, J., Majkráková, M., **Bucha**, **B.**, Zahorec, P., 2013: Modern methods for determinations of physical heights. In: *10th Slovak Geophysical Conference: Slovak Geophysical conference*, Smolenice, Slovakia, August 19–21, p. 49–50, ISBN 978-80-85754-27-8.

Citations

Citations registered in the Scopus database (09 May 2016).

Bucha, **B.**, Janák, J., 2013: A MATLAB-based graphical user interface program for computing functionals of the geopotential up to ultra-high degrees and orders. *Computers and Geosciences*, 56:186-–196. doi: 10.1016/j.cageo.2013.03.012.

Pitoňák, M., Šprlák, M., Hamáčková, E., Novák, P., 2016: Regional recovery of the disturbing gravitational potential by inverting satellite gravitational gradients. *Geophysical Journal International*, 205:89–98. doi: 10.1093/gji/ggw008.

Rexer, M., Hirt, C., 2015: Ultra-high-degree surface spherical harmonic analysis using the Gauss–Legendre and the Driscoll/Healy quadrature theorem and application to planetary topography models of Earth, Mars and Moon. *Surveys in Geophysics*, 36:803–830. doi: 10.1007/s10712-015-9345-z.

Zhou, B., Wang, J., Zhao, B., 2015: Micromorphology characterization and reconstruction of sand particles using micro X-ray tomography and spherical harmonics. *Engineering Geology*, 184:126–137. doi: 10.1016/j.enggeo.2014.11.009.

Hirt, C., Rexer, M., 2014: Earth2014: 1 arc-min shape, topography, bedrock and ice-sheet models – Available as gridded data and degree-10,800 spherical harmonics. *International Journal of Applied Earth Observation and Geoinformation*, 39:103–112. doi: 10.1016/j.jag.2015.03.001.

Hirt, C., Kuhn, M., 2014: Band-limited topographic mass distribution generates full-spectrum gravity field: Gravity forward modeling in the spectral and spatial domains revisited. *Journal of Geophysical Research: Solid Earth*, 119:3646–3661. doi: 10.1002/2013JB010900.

Bucha, **B.**, Janák, J., 2014: A MATLAB-based graphical user interface program for computing functionals of the geopotential up to ultra-high degrees and orders: Efficient computation at irregular surfaces. *Computers and Geosciences*, 66:219–227. doi: 10.1016/j.cageo.2014.02.005.

Hirt, C., Rexer, M., Schneinert, M., Pail, R., Claessens, S., Holmes, S., 2016: A new degree-2190 (10 km resolution) gravity field model for Antarctica developed from GRACE, GOCE and Bedmap2 data. *Journal of Geodesy*, 90:105–127. doi: 10.1007/s00190-015-0857-6.